C^2 Hermite Interpolation by Minkowski Pythagorean Hodograph Curves and Medial Axis Transform Approximation

Jiří Kosinka

Centre of Mathematics for Applications, University of Oslo, P.O. Box 1053, Blindern, 0316 Oslo

Zbyněk Šír*

Faculty of Mathematics and Physics, Charles University in Prague, Sokolovská 83, 186 75 Praha 8

Abstract

We describe and fully analyze an algorithm for C^2 Hermite interpolation by Pythagorean hodograph curves of degree 9 in Minkowski space $\mathbb{R}^{2,1}$. We show that for any data there exists a four-parameter system of interpolants and we identify the one which preserves symmetry and planarity of the input data and which has the optimal approximation degree. The new algorithm is applied to an efficient approximation of segments of the medial axis transform of a planar domain leading to rational parameterizations of the offsets of the domain boundaries with a high order of approximation.

Key words: Hermite interpolation, Pythagorean Hodograph curve, Medial axis transform, Minkowski space

1. Introduction

Pythagorean hodograph (PH) curves form an important subclass of polynomial parametric curves. The distinguishing property is that their arc length function is piecewise polynomial and, in the planar case, they possess rational offset curves. Since their introduction by Farouki and Sakkalis [13], planar and spatial PH curves have been thoroughly studied, see [9, 10] and the references cited therein.

Minkowski Pythagorean hodograph (MPH) curves were introduced by Choi et al. and Moon [6, 20]. The motivation is to describe the segments of the medial axis transform (cf. [8, 21]) of a planar domain: if the medial axis transform is a (collection of) MPH curves, then the boundary curve of the associated planar domain is a piecewise rational curve. As an important advantage, this property is shared by all offsets of the boundary.

PH and MPH curves possess certain similar aspects, which can be understood via a unifying framework designed in [7]. However, design algorithms for PH curves are much more numerous then those for MPH curves. We are particularly interested in Hermite interpolation algorithms in three dimensional space. G^1 Hermite interpolation using PH cubics in $\mathbb{R}^3$ [15] yields up to four interpolants. In the case of C^1 Hermite interpolation by spatial PH curves, one obtains a two-parameter family of quintics [11, 22]. There exists a particular interpolant which is geometrically invariant, preserves symmetry and planarity, and possesses approximation order 4. C^2 Hermite interpolation using PH curves of degree 9 in $\mathbb{R}^3$ gives a four-parameter family of interpolants [23]. The results are similar to the C^1 case, but now with approximation order 6.

In the case of MPH curves, G^1 Hermite interpolation using cubics was studied in [17]. Provided that the data are taken from a space-like curve without inflections, it yields up to four interpolants and one of them possesses approximation order 4. It is known that PH and MPH cubics are equivalent to cubic helices in Euclidean and Minkowski space, respectively, cf. [12, 16]. A $C^{1/2}$ interpolation scheme using MPH quartics has been discussed in [19]. A two-parameter family of MPH quintics interpolating given C^1 Hermite data was constructed in [18].

*Corresponding author

Email addresses: Jiri.Kosinka@cma.uio.no (Jiří Kosinka), Zbynek.Sir@mff.cuni.cz (Zbyněk Šír)

In the present paper we analyze a C^2 Hermite interpolation scheme for MPH nonics with the help of the unified approach via Clifford algebras [7]. Using the so called PH representation map we show that for the construction of MPH interpolants a sequence of linear and quadratic equations needs to be solved (similarly to the Euclidean case). Using the Clifford algebra formalism, we explicitly construct a four-parameter family of interpolants. Moreover, we identify the one that preserves certain symmetries and possesses the best approximation order. Higher order continuities are required when dealing with medial axis. It was shown in [1, 2] that matching domain boundary with C^2 continuity is crucial for the approximation stability of medial axis computation.

The remainder of this paper is organized as follows. Section 2 recalls some basic facts about Minkowski space, its associated Clifford algebra, medial axis transform and Minkowski Pythagorean hodograph curves. The C^2 Hermite interpolation algorithm is presented in Section 3. Since this algorithm yields a four-parameter system of interpolants, Section 4 focuses on the identification of a particular interpolant which is most suitable for applications. Finally, the paper is concluded with a discussion of applications of the presented algorithm and several examples in Section 5.

2. Preliminaries

In this section we recall basic facts about Minkowski space, Clifford algebra and Minkowski Pythagorean Hodograph curves.

2.1. Minkowski space and Lorentz transforms

The three-dimensional *Minkowski space* $\mathbb{R}^{2,1}$ is a three-dimensional real affine space equipped with the indefinite inner product defined by the matrix

$$G = (G_{i,j})_{i,j=1,2,3} = \text{diag}(1, 1, -1). \tag{1}$$

The inner product of two vectors $\mathbf{u} = (u_1, u_2, u_3)^\top$, $\mathbf{v} = (v_1, v_2, v_3)^\top$ is given by

$$\langle \mathbf{u}, \mathbf{v} \rangle = \mathbf{u}^\top G \mathbf{v} = u_1 v_1 + u_2 v_2 - u_3 v_3. \tag{2}$$

As the quadratic form associated with G is not definite, the squared norm of a vector, which is defined by $||\mathbf{v}||^2 = \langle \mathbf{v}, \mathbf{v} \rangle$ can be positive, negative or zero. A vector $\mathbf{v}$ is said to be *space-like* if $||\mathbf{v}||^2 > 0$, *time-like* if $||\mathbf{v}||^2 < 0$, and *light-like* (or isotropic) if $||\mathbf{v}||^2 = 0$. A *unit vector* $\mathbf{v} \in \mathbb{R}^{2,1}$ satisfies $||\mathbf{u}||^2 = \pm 1$. By scaling, space-like vectors $\mathbf{u}$ can be normalized to satisfy $||\mathbf{u}||^2 = 1$, and time-like ones to satisfy $||\mathbf{u}||^2 = -1$. A plane in Minkowski space is called space-, time- or light-like if the restriction of the quadratic form defined by G on this plane is positive definite, indefinite non degenerate or degenerate, respectively.

A linear mapping $L : \mathbb{R}^{2,1} \to \mathbb{R}^{2,1}$ is called a *Lorentz transform* if it preserves the Minkowski inner product, i.e., $\langle \mathbf{u}, \mathbf{v} \rangle = \langle L\mathbf{u}, L\mathbf{v} \rangle$ for all $\mathbf{u}, \mathbf{v} \in \mathbb{R}^{2,1}$. Lorentz transforms form the *Lorentz group* $\mathcal{L} = O(2, 1)$. Any Lorentz transform is described by a 3×3 matrix $L = (l_{i,j})_{i,j=1,2,3}$. Its column vectors $\mathbf{l}_1$, $\mathbf{l}_2$ and $\mathbf{l}_3$ satisfy $\langle \mathbf{l}_i, \mathbf{l}_j \rangle = G_{i,j}$, $i, j \in \{1, 2, 3\}$, i.e., they form an orthonormal basis of $\mathbb{R}^{2,1}$ with respect to the inner product (2). The equation $\langle \mathbf{l}_3, \mathbf{l}_3 \rangle = G_{3,3} = -1$ implies $l_{33}^2 \geq 1$. The Lorentz transform L is said to be *orthochronous* if $l_{33} \geq 1$. Obviously, the determinant of any Lorentz transform L equals to ± 1. The *special* ones are characterized by $\det(L) = 1$.

The Lorentz group $\mathcal{L}$ consists of four components. The special orthochronous Lorentz transforms form the subgroup $SO_+(2, 1)$. The remaining three components are $T_1 \cdot SO_+(2, 1)$, $T_2 \cdot SO_+(2, 1)$ and $T_1 \cdot T_2 \cdot SO_+(2, 1)$, where $T_1 = \text{diag}(1, 1, -1)$ and $T_2 = \text{diag}(1, -1, 1)$. Any special orthochronous Lorentz transform $L \in SO_+(2, 1)$ can be represented as $L = R(\alpha_1)H(\beta)R(\alpha_2)$, where

$$R(\alpha) = \begin{pmatrix} \cos\alpha & -\sin\alpha & 0 \\ \sin\alpha & \cos\alpha & 0 \\ 0 & 0 & 1 \end{pmatrix} \text{ and } H(\beta) = \begin{pmatrix} 1 & 0 & 0 \\ 0 & \cosh\beta & \sinh\beta \\ 0 & \sinh\beta & \cosh\beta \end{pmatrix} \tag{3}$$

are a planar rotation with angle α, and a *hyperbolic rotation* with angle β, respectively.

2.2. The Clifford algebra $\mathcal{C}\ell(2,1)$

Any real linear space $\mathbb{V}$, which is equipped with a quadratic form Q, has an associated *Clifford algebra*, defined as

$$\mathcal{C}\ell = T(\mathbb{V})/\langle \mathbf{v}\otimes\mathbf{v} - Q(\mathbf{v})\mathbf{1}\rangle, \tag{4}$$

i.e., as the quotient of the tensor algebra and its ideal forcing the equality $\mathbf{v}\otimes\mathbf{v} = Q(\mathbf{v})$, see [7] for a more detailed introduction. In particular we are interested in the Clifford algebra $\mathcal{C}\ell = \mathcal{C}\ell(2,1)$, which corresponds to the Minkowski space $\mathbb{R}^{2,1}$ i.e., to the three-dimensional real linear space with the indefinite quadratic form (2).

This Clifford algebra has real dimension 8 and has the following basis elements: the *scalar* identity element $\mathbf{1}$, the orthonormal basis *vectors* $\mathbf{e}_1$, $\mathbf{e}_2$, $\mathbf{e}_3$, the *bivectors* $\mathbf{e}_1\mathbf{e}_2$, $\mathbf{e}_2\mathbf{e}_3$, $\mathbf{e}_3\mathbf{e}_1$ and the *pseudo-scalar* $\mathbf{e}_1\mathbf{e}_2\mathbf{e}_3$. Any element of the Clifford algebra is a linear combination of these basis elements

$$\mathcal{A} \;=\; a_0\mathbf{1} + a_1\mathbf{e}_1 + a_2\mathbf{e}_2 + a_3\mathbf{e}_3 + a_4\mathbf{e}_1\mathbf{e}_2 + a_5\mathbf{e}_2\mathbf{e}_3 + a_6\mathbf{e}_3\mathbf{e}_1 + a_7\mathbf{e}_1\mathbf{e}_2\mathbf{e}_3. \tag{5}$$

The rules governing the non-commutative multiplication $\cdot$ can be deduced from the basic relations $\mathbf{e}_1^2 = \mathbf{e}_2^2 = \mathbf{1} = -\mathbf{e}_3^2$ and $\mathbf{e}_i\cdot\mathbf{e}_j = -\mathbf{e}_j\cdot\mathbf{e}_i$ if $i\neq j$. For any element $\mathcal{A}\in\mathcal{C}\ell$ we define its *conjugation* $\bar{\mathcal{A}}$ and *Clifford norm* as

$$\begin{aligned}\bar{\mathcal{A}} &= a_0\mathbf{1} - a_1\mathbf{e}_1 - a_2\mathbf{e}_2 - a_3\mathbf{e}_3 - a_4\mathbf{e}_1\mathbf{e}_2 - a_5\mathbf{e}_2\mathbf{e}_3 - a_6\mathbf{e}_3\mathbf{e}_1 + a_7\mathbf{e}_1\mathbf{e}_2\mathbf{e}_3,\\ N(\mathcal{A}) &= A\cdot\bar{A} = (a_0^2 - a_1^2 - a_2^2 + a_3^2 + a_4^2 - a_5^2 - a_6^2 + a_7^2) + (2a_0a_7 - 2a_1a_5 - 2a_2a_6 - 2a_3a_4)\mathbf{e}_1\mathbf{e}_2\mathbf{e}_3.\end{aligned} \tag{6}$$

The operation of conjugation satisfies $\overline{\mathcal{A}\cdot\mathcal{B}} = \bar{\mathcal{B}}\cdot\bar{\mathcal{A}}$. The algebra $\mathcal{C}\ell$ has the natural grading

$$\mathcal{C}\ell^0 = \mathbb{R}\mathbf{1},\quad \mathcal{C}\ell^1 = \mathbb{R}\mathbf{e}_1 + \mathbb{R}\mathbf{e}_2 + \mathbb{R}\mathbf{e}_3,\quad \mathcal{C}\ell^2 = \mathbb{R}\mathbf{e}_1\mathbf{e}_2 + \mathbb{R}\mathbf{e}_2\mathbf{e}_3 + \mathbb{R}\mathbf{e}_3\mathbf{e}_1,\quad \mathcal{C}\ell^3 = \mathbb{R}\mathbf{e}_1\mathbf{e}_2\mathbf{e}_3. \tag{7}$$

A vector $\mathbf{v} = (\lambda,\mu,\nu)^\top$ of $\mathbb{R}^{2,1}$ will be identified with the element $\lambda\mathbf{e}_1 + \mu\mathbf{e}_2 + \nu\mathbf{e}_3$ of $\mathcal{C}\ell^1$. The set of scalars combined with bivectors forms the subalgebra of even degree elements $\mathcal{C}\ell^+ = \mathcal{C}\ell^0\oplus\mathcal{C}\ell^2$.

We define the multiplicative group Spin as the set of all unit elements of $\mathcal{C}\ell^+$:

$$\mathrm{Spin} := \{\mathcal{A}\in\mathcal{C}\ell^+ : N(\mathcal{A}) = \pm 1\}.$$

This group has the action T on $\mathcal{C}\ell$ defined by

$$T(\mathcal{A})(\mathcal{B}) = \mathcal{A}\cdot\mathcal{B}\cdot\bar{\mathcal{A}}, \tag{8}$$

and stabilizes $\mathcal{C}\ell^1$, i.e., if $\mathbf{v}\in\mathcal{C}\ell^1 = \mathbb{R}^{2,1}$ then also $T(\mathcal{A})(\mathbf{v})\in\mathcal{C}\ell^1$. In fact the resulting transformation

$$T(\mathcal{A}) : \mathbb{R}^{2,1}\to\mathbb{R}^{2,1}$$

is a special Lorenz transform. More precisely, we have the natural exact sequence

$$1\to\{\pm 1\}\to\mathrm{Spin}\to SO(2,1)\to 1,$$

i.e., each element of $SO(2,1)$ corresponds to two elements of Spin differing only by the sign.

We define a commutative multiplication on $\mathcal{C}\ell^+\times\mathcal{C}\ell^+\to\mathcal{C}\ell^1$ by

$$\mathcal{A}\star\mathcal{B} = \frac{1}{2}(\mathcal{A}\cdot\mathbf{e}_1\cdot\bar{\mathcal{B}} + \mathcal{B}\cdot\mathbf{e}_1\cdot\bar{\mathcal{A}}). \tag{9}$$

Corresponding 2nd powers will be denoted $\mathcal{A}^{2\star}$. A direct computation shows that $\mathcal{A}\star\mathcal{B}$ indeed belongs to $\mathcal{C}\ell^1$. Note that for $\mathcal{A}\in\mathrm{Spin}$ we have $\mathcal{A}^{2\star} = T(\mathcal{A})(\mathbf{e}_1)$. Since no confusion is likely to arise, we simply omit the multiplication symbol $\cdot$ in the remainder of the paper.

2.3. Medial axis transform

Let $B_r(\mathbf{s})$ denote the disc in $\mathbb{R}^2$ with radius r centered at $\mathbf{s}$. For a given planar domain Ω the *medial axis transform* $\mathrm{MAT}(\Omega)$ is given by

$$\mathrm{MAT}(\Omega) := \{(\mathbf{s}, r) \in \Omega \times \mathbb{R}^+ : B_r(\mathbf{s}) \text{ is maximal in } \Omega\} \tag{10}$$

and the *medial axis* $\mathrm{MA}(\Omega)$ is the projection of $\mathrm{MAT}(\Omega)$ to $\mathbb{R}^2$, i.e., the set of centers of maximal discs. A disc in Ω is maximal if and only if it touches the boundary in at least two points (counting with multiplicity). This leads to a natural extension of $\mathrm{MAT}(\Omega)$ and $\mathrm{MA}(\Omega)$ to non-closed shapes. For example for two curves the MAT would be the set of all discs touching both of them and MA is their bisector. In the sequel we will use notions MA and MAT in this generalized sense.

If we have the MAT, the original domain boundary can be reconstructed as the envelope of corresponding discs. In particular, for a C^1 segment $\mathbf{p}(t) = (x(t), y(t), r(t))^\top \subset \mathrm{MAT}$ we can compute the corresponding boundary from the envelope formula (see [4])

$$(\tilde{x}(t), \tilde{y}(t))^\top = (x(t), y(t))^\top - \frac{r(t)r'(t)}{x'(t)^2 + y'(t)^2}(x'(t), y'(t))^\top \pm \frac{r(t)\sqrt{x'(t)^2 + y'(t)^2 - r'(t)}}{x'(t)^2 + y'(t)^2}(-y'(t), x'(t))^\top. \tag{11}$$

The term $\sqrt{x'(t)^2 + y'(t)^2 - r'(t)}$ can be interpreted as the Minkowski norm of the curve derivative $\mathbf{p}'$, which leads to considering $\mathbb{R}^{2,1}$ as the natural ambient space for MAT.

2.4. Minkowski Pythagorean hodograph curves

Recall that a polynomial curve in Euclidean space is called a *Pythagorean hodograph* (PH) curve (cf. [9]), if the squared norm of its first derivative (or hodograph) is the square of another polynomial. Following [20], *Minkowski Pythagorean hodograph* (MPH) curves are defined similarly, but with respect to the norm induced by the Minkowski inner product. More precisely, a polynomial curve $\mathbf{p} \in \mathbb{R}^{2,1}$, $\mathbf{p} = (x, y, r)^\top$ is called an MPH curve if

$$||\mathbf{p}'||^2 = x'^2 + y'^2 - r'^2 = \sigma^2 \tag{12}$$

for some polynomial σ.

As observed in [6, 20], if the medial axis transform of a planar domain is (a collection of) MPH curve(s), then the coordinate functions of the corresponding boundary curves (i.e., the envelopes of the discs with centers (x, y) and radius r) are (piecewise) rational functions. Due to the definition of MPH curves, the tangent vector $\mathbf{p}'(t)$ cannot be time-like. Also, light-like tangent vectors correspond to roots of the polynomial σ in (12), see [21, Section 2.1] for more details.

According to [20], the equation (12) holds if and only if there exist polynomials $u(t)$, $v(t)$, $p(t)$ and $q(t)$ such that

$$\begin{aligned} x'(t) &= u(t)^2 - v(t)^2 - p(t)^2 + q(t)^2, \\ y'(t) &= -2(u(t)v(t) + p(t)q(t)), \\ r'(t) &= 2(u(t)q(t) + v(t)p(t)), \\ \sigma(t) &= u(t)^2 + v(t)^2 - p(t)^2 - q(t)^2. \end{aligned} \tag{13}$$

This result can be reformulated using Clifford algebra $\mathcal{C}\ell(2, 1)$, see [7].

Lemma 1. *A polynomial curve $\mathbf{p}(t)$ in $\mathbb{R}^{2,1}$ is an MPH curve if and only if there exists a polynomial curve $\mathcal{A}(t) = u(t) + v(t)\mathbf{e}_1\mathbf{e}_2 + p(t)\mathbf{e}_2\mathbf{e}_3 + q(t)\mathbf{e}_3\mathbf{e}_1$ in the subalgebra $\mathcal{C}\ell^+$ such that*

$$\mathbf{p}'(t) = \mathbf{h}(t) = \mathcal{A}(t)\mathbf{e}_1\bar{\mathcal{A}}(t) = \mathcal{A}(t)^{2\star}. \tag{14}$$

Consequently, the construction of MPH curves is reduced to the construction of a suitable curve $\mathcal{A}(t)$ in the subalgebra $\mathcal{C}\ell^+$, which will be called the *preimage* curve.

We will use MPH curves of degree 9. The MPH curves, their hodograph $\mathbf{h}(t) = \mathbf{p}'(t)$ and the preimage $\mathcal{A}(t)$ will be expressed in the Bernstein-Bézier representation [14]

$$\mathbf{p}(t) = \sum_{i=0}^{9} \mathbf{p}_i B_i^9(t),\ \mathbf{h}(t) = \sum_{i=0}^{8} \mathbf{h}_i B_i^8(t),\ \mathcal{A}(t) = \sum_{i=0}^{4} \mathcal{A}_i B_i^4(t),\ t \in [0, 1], \tag{15}$$

where $\mathbf{p}_i$, $\mathbf{h}_i$ (pure vectors) and $\mathcal{A}_i \in \mathcal{C}\ell^+$ are the control points and $B_j^n(t)$ are the Bernstein polynomials. The relation between the hodograph and the preimage $\mathbf{h}(t) = \mathcal{A}(t)^{2\star}$ can be expressed using the control points as

$$\mathbf{h}_0 = \mathcal{A}_0^{2\star}, \qquad \mathbf{h}_8 = \mathcal{A}_4^{2\star}, \tag{16}$$
$$\mathbf{h}_1 = \mathcal{A}_0 \star \mathcal{A}_1, \qquad \mathbf{h}_7 = A_3 \star \mathcal{A}_4, \tag{17}$$
$$\mathbf{h}_2 = (4\mathcal{A}_1^{2\star} + 3\mathcal{A}_0 \star \mathcal{A}_2)/7, \qquad \mathbf{h}_6 = (4\mathcal{A}_3^{2\star} + 3\mathcal{A}_2 \star \mathcal{A}_4)/7, \tag{18}$$
$$\mathbf{h}_3 = (\mathcal{A}_0 \star \mathcal{A}_3 + 6\mathcal{A}_1 \star \mathcal{A}_2)/7, \qquad \mathbf{h}_5 = (\mathcal{A}_1 \star \mathcal{A}_4 + 6\mathcal{A}_2 \star \mathcal{A}_3)/7, \tag{19}$$
$$\mathbf{h}_4 = (18\mathcal{A}_2^{2\star} + \mathcal{A}_0 \star \mathcal{A}_4 + 16\mathcal{A}_1 \star \mathcal{A}_3)/35. \tag{20}$$

The MPH curve is then obtained by integrating the hodograph and it possesses the control points

$$\mathbf{p}_j = \mathbf{p}_0 + \frac{1}{9}\sum_{i=0}^{j-1} \mathbf{h}_i, \quad j = 1, \ldots, 9. \tag{21}$$

3. C^2 Hermite interpolation by Minkowski Pythagorean hodograph curves

In this section we first give solutions to certain equations in $\mathcal{C}\ell(2,1)$. Then we show that the interpolation problem can be reduced to solving a sequence of these equations. Finally, we construct all interpolants to given C^2 data.

3.1. Elementary equations in $\mathcal{C}\ell(2,1)$

Lemma 2. *Let* $\mathbf{v}$ *be a pure vector and* $\mathcal{A} \in \mathcal{C}\ell^+$ *such that* $N(\mathcal{A}) \neq 0$. *Then all solutions of the linear equation*

$$\mathcal{X} \star \mathcal{A} = \mathbf{v} \tag{22}$$

form the one-parameter family

$$\mathcal{X}_\tau = \frac{(\mathbf{v} + \tau\mathbf{e}_1\mathbf{e}_2\mathbf{e}_3)\mathcal{A}\mathbf{e}_1}{N(\mathcal{A})}, \quad \tau \in \mathbb{R}. \tag{23}$$

PROOF. We can write

$$\mathcal{X} \star \mathcal{A} = \frac{1}{2}(\mathcal{X}\mathbf{e}_1\bar{\mathcal{A}} + \mathcal{A}\mathbf{e}_1\bar{\mathcal{X}}) = \frac{1}{2}(\mathcal{X}\mathbf{e}_1\bar{\mathcal{A}} - \overline{\mathcal{X}\mathbf{e}_1\bar{\mathcal{A}}}) = \mathcal{X}\mathbf{e}_1\bar{\mathcal{A}} - \tau\mathbf{e}_1\mathbf{e}_2\mathbf{e}_3. \tag{24}$$

The last equality holds since $\mathcal{X}\mathbf{e}_1\bar{\mathcal{A}}$ contains only vector part, which changes sign under conjugation, and the pseudoscalar part $\tau\mathbf{e}_1\mathbf{e}_2\mathbf{e}_3$, which does not change sign under conjugation and therefore cancels out. Thus, (22) becomes

$$\mathcal{X}\mathbf{e}_1\bar{\mathcal{A}} = \mathbf{v} + \tau\mathbf{e}_1\mathbf{e}_2\mathbf{e}_3 \tag{25}$$

and multiplying it from right by $\mathcal{A}\mathbf{e}_1$ leads to the result. □

Definition 1. *The subgroup of elements of* Spin *stabilizing the element* $\mathbf{e}_1$ *will be denoted by* Spin_1*:*

$$\mathrm{Spin}_1 = \{\mathcal{W} \in \mathrm{Spin} : \mathcal{W}\mathbf{e}_1\bar{\mathcal{W}} = \mathbf{e}_1\}.$$

Moreover, we have the commutative subgroup

$$\mathrm{Spin}_1^+ = \{\mathcal{W} \in \mathrm{Spin}_1 : N(\mathcal{W}) = 1\}.$$

The following result is proved in Lemma 1 of [18].

Lemma 3.

$$\mathrm{Spin}_1^+ = \{\pm\cosh(\phi) - \sinh(\phi)\,\mathbf{e}_2\mathbf{e}_3,\ \phi \in \mathbb{R}\} \tag{26}$$
$$\mathrm{Spin}_1 = \mathrm{Spin}_1^+ \cup \{-\sinh(\phi)\,\mathbf{e}_1\mathbf{e}_2 \pm \cosh(\phi)\,\mathbf{e}_3\mathbf{e}_1,\ \phi \in \mathbb{R}\}. \tag{27}$$

For any space-like or light-like vector $\mathbf{v} = (\lambda, \mu, \nu)^\top$ define

$$\alpha(\mathbf{v}) := \frac{1}{2}(\lambda + ||\mathbf{v}||) \quad \text{and} \quad \sqrt{\mathbf{v}} := -\frac{(\mathbf{v} + ||\mathbf{v}||\mathbf{e}_1)\mathbf{e}_3}{2\sqrt{|\alpha(\mathbf{v})|}}. \tag{28}$$

A direct computation leads to

Lemma 4. *For any space-like or light-like vector* $\mathbf{v}$ *we have*

$$\sqrt{\mathbf{v}}\mathbf{e}_1\overline{\sqrt{\mathbf{v}}} = \mathrm{sgn}(\alpha(\mathbf{v}))\mathbf{e}_1.$$

Lemma 5. *Let* $\mathbf{v}$ *be a space-like or light-like vector. All solutions of the equation*

$$\mathcal{X}^{2\star} = \mathbf{v} \tag{29}$$

are of the form

$$\begin{array}{rcll} \mathcal{X}_\mathcal{W} & = & \sqrt{\mathbf{v}}\mathcal{W}, & \text{for } \alpha(\mathbf{v}) > 0 \text{ and} \\ \mathcal{X}_\mathcal{W} & = & \sqrt{\mathbf{v}}\mathbf{e}_2\mathbf{e}_3\mathcal{W}, & \text{for } \alpha(\mathbf{v}) < 0, \end{array} \tag{30}$$

where $\mathcal{W} \in \mathrm{Spin}_1$.

PROOF. Recall that $\mathcal{X}^{2\star} := \mathcal{X}\mathbf{e}_1\bar{\mathcal{X}}$. By Lemma 4 we have that $\sqrt{\mathbf{v}}$ (resp. $\sqrt{\mathbf{v}}\mathbf{e}_2\mathbf{e}_3$) is a solution of (29) since $\mathbf{e}_2\mathbf{e}_3\mathbf{e}_1\overline{\mathbf{e}_2\mathbf{e}_3} = -\mathbf{e}_1$. Moreover, elements of Spin_1 are exactly the solutions of the equation $\mathcal{W}\mathbf{e}_1\bar{\mathcal{W}} = \mathbf{e}_1$, which concludes the proof. □

Remark 1. The case $\alpha(\mathbf{v}) = 0$ leads to a different one-parameter system of solutions and we exclude this case in order to simplify the presentation. As we shall see later in Section 4.2, the case $\alpha(\mathbf{v}) = 0$ does not occur if the data are sampled from a space-like C^∞ curve with a sufficiently small step-size.

Lemma 6. *The systems of solutions* (23) *and* (30) *are equivariant with respect to the action of* Spin_1^+ *in the following special sense. Suppose that some data* $\mathbf{v}$, $\mathcal{A}$ *enter equations* (22) *and* (29) *yielding the systems of solutions* $\mathcal{X}_\tau$, $\mathcal{X}_\mathcal{W}$. *Let for some* $\mathcal{V} \in \mathrm{Spin}_1^+$ *the transformed data* $\tilde{\mathbf{v}} = \mathcal{V}\mathbf{v}\bar{\mathcal{V}}$ *and* $\tilde{\mathcal{A}} = \mathcal{V}\mathcal{A}\mathcal{V}$ *give solutions* $\tilde{\mathcal{X}}_\tau$, $\tilde{\mathcal{X}}_\mathcal{W}$. *Then for any parameter* $\tau \in \mathbb{R}$ *or* $\mathcal{W} \in \mathrm{Spin}_1$ *we have*

$$\tilde{\mathcal{X}}_\tau = \mathcal{V}\mathcal{X}_\tau\mathcal{V}, \quad \tilde{\mathcal{X}}_\mathcal{W} = \mathcal{V}\mathcal{X}_\mathcal{W}\mathcal{V}. \tag{31}$$

PROOF. Note that $\mathcal{V}\mathbf{v}\bar{\mathcal{V}}$ is a hyperbolic rotation of $\mathbf{v}$ about the $\mathbf{e}_1$ axis and so $||\tilde{\mathbf{v}}|| = ||\mathbf{v}||$ and $\alpha(\tilde{\mathbf{v}}) = \alpha(\mathbf{v})$. Also, $\mathcal{V}\bar{\mathcal{V}} = 1$ and $N(\tilde{\mathcal{A}}) = N(\mathcal{A})$. Moreover, $\mathcal{V}$ commutes with $\mathbf{e}_1$, $\mathbf{e}_2\mathbf{e}_3$ and $\mathbf{e}_1\mathbf{e}_2\mathbf{e}_3$ and we also have $\mathbf{e}_3 = \mathcal{V}\mathbf{e}_3\mathcal{V}$. Using these facts we can write

$$\tilde{\mathcal{X}}_\tau = \frac{(\tilde{\mathbf{v}} + \tau\mathbf{e}_1\mathbf{e}_2\mathbf{e}_3)\tilde{\mathcal{A}}\mathbf{e}_1}{N(\tilde{\mathcal{A}})} = \frac{(\mathcal{V}\mathbf{v}\bar{\mathcal{V}} + \tau\mathbf{e}_1\mathbf{e}_2\mathbf{e}_3)\mathcal{V}\mathcal{A}\mathcal{V}\mathbf{e}_1}{N(\mathcal{A})} = \mathcal{V}\frac{(\mathbf{v} + \tau\mathbf{e}_1\mathbf{e}_2\mathbf{e}_3)\mathcal{A}\mathbf{e}_1}{N(\mathcal{A})}\mathcal{V} = \mathcal{V}\mathcal{X}_\tau\mathcal{V}. \tag{32}$$

Similarly we have

$$\sqrt{\tilde{\mathbf{v}}} = -\frac{(\mathcal{V}\mathbf{v}\bar{\mathcal{V}} + ||\mathbf{v}||\mathbf{e}_1)\mathbf{e}_3}{2\sqrt{|\alpha(\mathbf{v})|}} = -\frac{(\mathcal{V}\mathbf{v}\bar{\mathcal{V}} + ||\mathbf{v}||\mathcal{V}\mathbf{e}_1\bar{\mathcal{V}})\mathcal{V}\mathbf{e}_3\mathcal{V}}{2\sqrt{|\alpha(\mathbf{v})|}} = \mathcal{V}\sqrt{\mathbf{v}}\mathcal{V}. \tag{33}$$

Since the choice of solution does not change in (30) and $\mathcal{V}$ commutes with $\mathcal{W}$ and $\mathbf{e}_2\mathbf{e}_3$, we obtain (31). □

3.2. System of solutions to the C^2 Hermite interpolation problem

We construct a spatial MPH curve $\mathbf{p}(t)$ which matches given C^2 Hermite boundary data. More precisely, the curve is to interpolate the end points $\mathbf{p}_b$, $\mathbf{p}_e$, the first derivative vectors (velocities) $\mathbf{v}_b$, $\mathbf{v}_e$ and the second derivative vectors (accelerations) $\mathbf{a}_b$, $\mathbf{a}_e$.

In all we have 18 scalar conditions. Three of them are satisfied by choosing the first control point of the curve $\mathbf{p}_0 = \mathbf{p}_b$. The remaining 15 conditions must be satisfied by determining the control points of the preimage. As

the preimage has 4 components, apparently the 15 conditions could be satisfied by 4 control points leading to the preimage of degree 3 and MPH curves of degree 7. But our experiments showed that the resulting system of equations is highly nonlinear and does not have solutions for all input data. Therefore we will use MPH interpolants of degree 9, for which the problem always has solutions forming a four-parameter family.

Two curves $\mathbf{p}(t)$, $\tilde{\mathbf{p}}(t)$ share the same hodograph if and only if they differ only by a translation. Consequently, a spatial MPH curve $\mathbf{p}(t)$ is fully determined by the preimage $\mathcal{A}(t)$ and by the location of its starting point $\mathbf{p}(0)$.

Using curves of degree 9, the interpolation conditions lead to the equations

$$\mathbf{h}_0 = \mathbf{v}_b,\ \mathbf{h}_8 = \mathbf{v}_e,\ 8(\mathbf{h}_1 - \mathbf{h}_0) = \mathbf{a}_b,\ 8(\mathbf{h}_8 - \mathbf{h}_7) = \mathbf{a}_e, \tag{34}$$

$$\frac{1}{9}\sum_{i=0}^{8} \mathbf{h}_i = (\mathbf{p}_e - \mathbf{p}_b). \tag{35}$$

Substituting into (16)-(20), this last equation, after some simplifications, becomes

$$\begin{aligned}&(12\mathcal{A}_2 + 10\mathcal{A}_1 + 5\mathcal{A}_0 + 5\mathcal{A}_4 + 10\mathcal{A}_3)^{2\star} = \\ &2520(\mathbf{p}_e - \mathbf{p}_b) - 435(\mathbf{v}_e + \mathbf{v}_b) + \tfrac{45}{2}(\mathbf{a}_e - \mathbf{a}_b) \\ &-(60\mathcal{A}_1^{2\star} - 60\mathcal{A}_0 \star \mathcal{A}_3 - 60\mathcal{A}_1 \star \mathcal{A}_4 + 60\mathcal{A}_3^{2\star} - 42\mathcal{A}_0 \star \mathcal{A}_4 - 72\mathcal{A}_1 \star \mathcal{A}_3).\end{aligned} \tag{36}$$

The construction of MPH interpolants.

1. Compute the control points $\mathbf{h}_0$, $\mathbf{h}_1$, $\mathbf{h}_7$ and $\mathbf{h}_8$ from (34).
2. The control points $\mathcal{A}_0$, $\mathcal{A}_4$ can be computed using equations (16), which are of type (29) and therefore each of $\mathcal{A}_0$, $\mathcal{A}_4$ depends on one free parameter, $\mathcal{W}_0 \in \mathrm{Spin}_1$ and $\mathcal{W}_4 \in \mathrm{Spin}_1$.
3. The control points $\mathcal{A}_1$, $\mathcal{A}_3$ can be computed from equations (17), which are of type (22). The control point $\mathcal{A}_1$ depends on the parameter $\mathcal{W}_0$ via $\mathcal{A}_0$ and on a new parameter τ_1. Similarly $\mathcal{A}_3$ depends on the parameter $\mathcal{W}_4$ via $\mathcal{A}_4$ and on a new parameter τ_3.
4. The control point $\mathcal{A}_2$ can be computed from (36), which is essentially of type (29). This control point will depend on all previous control points and therefore on all parameters $\mathcal{W}_0$, $\mathcal{W}_4$, τ_1 and τ_3 and on a new parameter $\mathcal{W}_2 \in \mathrm{Spin}_1$.
5. Compute control points $\mathbf{h}_2$, $\mathbf{h}_3$, $\mathbf{h}_4$, $\mathbf{h}_5$, $\mathbf{h}_6$ from equations (18)–(19), set $\mathbf{p}_0 = \mathbf{p}_b$ and compute the remaining control points of $\mathbf{p}(t)$ using equation (21).

Summing up, we arrive successively at families of suitable preimages $\mathcal{A}_\Phi(t)$, hodographs $\mathbf{h}_\Phi(t)$ and PH curves $\mathbf{p}_\Phi(t)$ depending on the parameter vector $\Phi = [\mathcal{W}_0, \tau_1, \mathcal{W}_2, \tau_3, \mathcal{W}_4]$. However, as in the cases of C^1 PH and MPH and C^2 PH Hermite interpolation [22, 23, 18], one of the parameters can be chosen due to the nontrivial fibers of the mapping $preimage \to hodograph$ (13), which are in fact isomorphic to the group Spin_1 as shows the following

Lemma 7. *Let $\mathbf{h}_\Phi$, where $\Phi = [\mathcal{W}_0, \tau_1, \mathcal{W}_2, \tau_3, \mathcal{W}_4]$, be the hodograph of a particular MPH interpolant to some given input data and let $\tilde{\Phi} = [\mathcal{W}_0\mathcal{W}, \tau_1, \mathcal{W}_2\mathcal{W}, \tau_3, \mathcal{W}_4\mathcal{W}]$ for some $\mathcal{W} \in \mathrm{Spin}_1$. Then*

$$\mathbf{h}_\Phi(t) = \mathbf{h}_{\tilde{\Phi}}(t). \tag{37}$$

PROOF. We claim that for all preimage control points we have $\mathcal{A}_i(\tilde{\Phi}) = \mathcal{A}_i(\Phi)\mathcal{W}$. This is immediately clear for $i = 0, 4$ due to the form of (30). The same relation holds for $i = 1, 3$ because $\mathcal{A}_0$ and $\mathcal{A}_4$ already enter suitably modified (multiplied by $\mathcal{W}$) into (23) for $\mathcal{A}_1$ and $\mathcal{A}_3$. Due to the equality $\mathcal{W}\mathbf{e}_1/N(\mathcal{W}) = \mathbf{e}_1\mathcal{W}$ the element $\mathcal{W}$ will appear only as a factor at the end of the expression. Similarly in the computation of $\mathcal{A}_2$ from formula (36), the factor $\mathcal{W}$ cancels out on the right-hand side and remains as a multiple on the left-hand side. Summing up we obtain $\mathcal{A}_\Phi(t)\mathcal{W} = \mathcal{A}_{\tilde{\Phi}}(t)$ yielding

$$\mathbf{h}_{\tilde{\Phi}}(t) = \mathcal{A}_i(\tilde{\Phi})\mathbf{e}_1\bar{\mathcal{A}}_i(\tilde{\Phi}) = \mathcal{A}_i(\Phi)\mathcal{W}\mathbf{e}_1\bar{\mathcal{W}}\bar{\mathcal{A}}_i(\Phi) = \mathbf{h}_\Phi(t), \tag{38}$$

as was to be shown. □

In particular, we can apply $\mathcal{W} = \mathcal{W}_2^{-1} = N(\mathcal{W}_2)\bar{\mathcal{W}}_2$ in Lemma 7, which leads to the simplified parameter vector $\Phi = [\tilde{\mathcal{W}}_0, \tau_1, \mathbf{1}, \tau_3, \tilde{\mathcal{W}}_4]$. For the remainder of the paper we will suppose this choice and omit the middle parameter. The four remaining parameters describe the system of Hermite interpolants fully.

4. Identifying a suitable interpolant

For practical purposes we need to identify one particular interpolant within the family $\mathbf{p}[\mathcal{W}_0, \tau_1, \tau_3, \mathcal{W}_4]$ that is suitable for applications. We use certain symmetry criteria and approximation order.

4.1. The parameterization and invariance of interpolants

For any given C^2 Hermite data $\mathbf{p}_0$, $\mathbf{p}_1$, $\mathbf{v}_0$, $\mathbf{v}_1$, $\mathbf{a}_0$ and $\mathbf{a}_1$ the system $\{\mathbf{p}_{[\mathcal{W}_0,\tau_1,\tau_3,\mathcal{W}_4]}(t)\}$ represents *all* MPH interpolants. Therefore, it is invariant with respect to Lorentz transforms. More precisely, if we apply a Lorentz transform L to the Hermite data, we obtain modified data $\tilde{\mathbf{p}}_0 = L(\mathbf{p}_0)$, $\tilde{\mathbf{p}}_1 = L(\mathbf{p}_1)$, $\tilde{\mathbf{v}}_0 = L(\mathbf{v}_0)$, $\tilde{\mathbf{v}}_1 = L(\mathbf{v}_1)$, $\tilde{\mathbf{a}}_0 = L(\mathbf{a}_0)$ and $\tilde{\mathbf{a}}_1 = L(\mathbf{a}_1)$ along with the modified interpolating MPH curves $\tilde{\mathbf{p}}_{[\bar{\mathcal{W}}_0,\bar{\tau}_1,\bar{\tau}_3,\bar{\mathcal{W}}_4]}(t)$ satisfying

$$\{\bar{\mathbf{p}}_{[\bar{\mathcal{W}}_0,\bar{\tau}_1,\bar{\tau}_3,\bar{\mathcal{W}}_4]}\} = L(\{\mathbf{p}_{[\mathcal{W}_0,\tau_1,\tau_3,\mathcal{W}_4]}(t)\}).$$

In general, however, the transform L does not preserve the parameterization of the interpolants by the free parameters. The relations $\bar{\mathcal{W}}_0 = \mathcal{W}_0$, $\bar{\tau}_1 = \tau_1$, $\bar{\tau}_3 = \tau_3$, $\bar{\mathcal{W}}_4 = \mathcal{W}_4$ are not always satisfied. Therefore, we must fix the parameterization of the family of interpolants by Φ using a canonical position of the data. In order to simplify our presentation we impose the following restrictions:

- We assume that the sum $\mathbf{t}_0+\mathbf{t}_1$ of the given boundary derivatives is a space-like vector. We need this assumption in order to define the standard position in a symmetric fashion. For instance, if the data are sampled from a space-like curve with some step size h, then this assumption is always satisfied provided that h is sufficiently small.
- We will only consider solutions given by the parameter vector $\Phi = [\mathcal{W}_0, \tau_1, \tau_3, \mathcal{W}_4]$ with $\mathcal{W}_0, \mathcal{W}_4 \in \mathrm{Spin}_1^+$. As we show below, this branch of interpolants contains the most suitable one.

General case can be still considered but would lead to a lengthy discussion of various cases without giving any substantial practical advantage.

Definition 2. *If $\mathbf{t}_0 + \mathbf{t}_1$ is a positive multiple of $\mathbf{e}_1$ and $\mathbf{p}_0 = \mathbf{0}$, then the input C^2 Hermite data are said to be in a* standard position. *We parameterize the MPH interpolants as follows. First, we transform the input data to a standard position applying a special orthochronous transform (see section 2.1). Then we construct the MPH interpolants $\mathbf{p}_{[\mathcal{W}_0,\tau_1,\tau_3,\mathcal{W}_4]}(t)$. Finally, we transform the solutions back to the original position. From now on, $\mathbf{p}_{[\mathcal{W}_0,\tau_1,\tau_3,\mathcal{W}_4]}(t)$ will denote the interpolant obtained in this way, i.e., the parameters $[\mathcal{W}_0, \tau_1, \tau_3, \mathcal{W}_4]$ are no longer applied to the original position of the data, but to the data transformed to a standard position.*

Note, that there are many standard positions differing by a hyperbolic rotation about the $\mathbf{e}_1$ axis. The following lemma ensures the correctness of the definition.

Lemma 8. *The parameterization $\mathbf{p}_{[\mathcal{W}_0,\tau_1,\tau_3,\mathcal{W}_4]}(t)$ is well defined, i.e., hyperbolic rotations preserving $\mathbf{e}_1$ do not affect this labeling.*

PROOF. Hyperbolic rotations about the $\mathbf{e}_1$ axis are represented within $\mathcal{C}\ell$ by $T(\mathcal{V})$, where $\mathcal{V} \in \mathcal{C}\ell^+$, i.e., by simultaneous multiplication by $\mathcal{V}$ from the left and by $\bar{\mathcal{V}}$ from the right. Suppose that we have some data $\mathbf{p}_0$, $\mathbf{p}_1$, $\mathbf{v}_0$, $\mathbf{v}_1$, $\mathbf{a}_0$ and $\mathbf{a}_1$ in a standard position and the interpolant $\mathbf{p}(t)$ is constructed using the parameter vector $[\mathcal{W}_0, \tau_1, \tau_3, \mathcal{W}_4]$. Let us construct the interpolant $\tilde{\mathbf{p}}$ with the same parameter vector to the rotated data $T(\mathcal{V})(\mathbf{p}_0)$, $T(\mathcal{V})(\mathbf{p}_1)$, $T(\mathcal{V})(\mathbf{v}_0)$, $T(\mathcal{V})(\mathbf{v}_1)$, $T(\mathcal{V})(\mathbf{a}_0)$ and $T(\mathcal{V})(\mathbf{a}_1)$. Let $\mathcal{A}_i$ denote the original preimage control points and $\tilde{\mathcal{A}}_i$ preimage control points for the rotated data. Due to Lemma 6 we have $\tilde{\mathcal{A}}_0 = \mathcal{V}\mathcal{A}_0\mathcal{V}$ and $\tilde{\mathcal{A}}_4 = \mathcal{V}\mathcal{A}_4\mathcal{V}$. This in turn leads to $\tilde{\mathcal{A}}_1 = \mathcal{V}\mathcal{A}_1\mathcal{V}$ and $\tilde{\mathcal{A}}_3 = \mathcal{V}\mathcal{A}_3\mathcal{V}$. Now, since

$$(\mathcal{V}\mathcal{A}\mathcal{V}) \star (\mathcal{V}\mathcal{B}\mathcal{V}) = \mathcal{V}(\mathcal{A} \star \mathcal{B})\bar{\mathcal{V}} \tag{39}$$

the right-hand side of (36) is suitably modified and we get $\tilde{\mathcal{A}}_3 = \mathcal{V}\mathcal{A}_3\mathcal{V}$. Summing up we have $\tilde{\mathcal{A}}(t) = \mathcal{V}\mathcal{A}(t)\mathcal{V}$ leading to $\tilde{\mathbf{p}} = \mathcal{V}(\mathbf{p})\bar{\mathcal{V}}$ due to (39). Thus the interpolants are transformed in the same way the input data are. □

As we will see below, the solution $\mathbf{p}_{[\mathbf{1},0,0,\mathbf{1}]}(t)$ demonstrates the best asymptotic behavior. Its suitability for applications is also confirmed by the following theorem. We state it without proof, which is purely technical.

Theorem 1. *The interpolant $\mathbf{p}[\mathbf{1}, 0, 0, \mathbf{1}](t)$ is symmetric with respect to reversion of the data and preserves planarity of planar data.*

4.2. Approximation order

We assume that a sufficiently smooth space-like curve $\mathbf{C}(T)$ in Minkowski space $\mathbb{R}^{2,1}$ is given. It may be a branch of the medial axis transform of a planar domain. In this situation, the curve is space-like, except for those end points, which correspond to vertices (curvature maxima) of the boundary of the domain.

In order to approximate this curve by a nonic MPH spline, we sample C^2 Hermite boundary data from segments $T \in [t_0, t_0+h]$ and apply the interpolation procedure. The following theorem analyzes the behavior of the error as the step size h tends to zero. We also point out that the results on the approximation order of the MAT imply analogous results for the Hausdorff distance of the associated planar domains, cf. Section 6.3 of [17].

Theorem 2. *If the step-size h is sufficiently small, then the interpolant $\mathbf{p}[\mathbf{1},0,0,\mathbf{1}](t)$ is well defined and has approximation order 6. All other interpolants with $\tau_1 = \tau_3 = 0$ for arbitrary but constant values of $\mathcal{W}_0$ and $\mathcal{W}_4$ have approximation order 1. Otherwise, the approximation order is equal to $\frac{1}{2}$.*

PROOF. We prove this theorem with the help of power series. Without loss of generality we set $\mathbf{C}(0) = (0,0,0)^\top$ and $\mathbf{C}'(0) = (1,0,0)^\top$, hence

$$\mathbf{C}(T) = (T + \sum_{i=2}^{\infty} \frac{x_i}{i!}T^i, \sum_{i=2}^{\infty} \frac{y_i}{i!}T^i, \sum_{i=2}^{\infty} \frac{r_i}{i!}T^i)^\top, \tag{40}$$

where x_i, y_i and r_i are arbitrary but fixed coefficients, $i = 2, 3, \ldots$. The Hermite interpolation procedure is applied to the segment $\mathbf{c}(t) = \mathbf{C}(th)$, $t \in [0,1]$, where the step-size h specifies the length.

In order to prove the theorem, we evaluate the Taylor expansions with respect to h of all quantities occurring in the interpolation algorithm, using a suitable computer algebra tool. Due to the space limitations and the complexity of the expressions we present only the leading terms of certain quantities.

First we generate the Taylor expansions of the Hermite boundary data,

$$\mathbf{p}_0 = \begin{pmatrix} 0 \\ 0 \\ 0 \end{pmatrix}, \qquad \mathbf{v}_0 = \begin{pmatrix} h \\ 0 \\ 0 \end{pmatrix}, \qquad \mathbf{a}_0 = \begin{pmatrix} x_2h^2 \\ y_2h^2 \\ r_2h^2 \end{pmatrix},$$

$$\mathbf{p}_1 = \begin{pmatrix} h + \frac{1}{2}x_2h^2 + \ldots \\ \frac{1}{2}y_2h^2 + \frac{1}{6}y_3h^3 + \ldots \\ \frac{1}{2}r_2h^2 + \frac{1}{6}r_3h^3 + \ldots \end{pmatrix}, \quad \mathbf{v}_1 = \begin{pmatrix} h + x_2h^2 + \ldots \\ y_2h^2 + \frac{1}{2}y_3h^3 + \ldots \\ r_2h^2 + \frac{1}{2}r_3h^3 + \ldots \end{pmatrix}, \quad \mathbf{a}_1 = \begin{pmatrix} x_2h^2 + x_3h^3 + \ldots \\ y_2h^2 + y_3h^3 + \ldots \\ r_2h^2 + r_3h^3 + \ldots \end{pmatrix}.$$

In order to transform these data into a standard position, we apply a special orthochronous Lorentz transform with the Taylor expansion

$$U = \begin{pmatrix} 1 - \frac{y_2^2 - r_2^2}{8}h^2 + \ldots & \frac{y_2}{2}h + \frac{y_3 - x_2y_2}{4}h^2 + \ldots & -\frac{r_2}{2}h - \frac{r_3 - x_2r_2}{4}h^2 + \ldots \\ -\frac{y_2}{2}h - \frac{y_3 - x_2y_2}{4}h^2 + \ldots & 1 - \frac{y_2^2}{8}h^2 + \ldots & 0 \\ -\frac{r_2}{2}h - \frac{r_3 - x_2r_2}{4}h^2 + \ldots & -\frac{y_2r_2}{4}h^2 + \ldots & 1 + \frac{r_2^2}{8}h^2 + \ldots \end{pmatrix}.$$

Then we compute the Taylor expansions of the control points of the preimage for the transformed data $U(\mathbf{p}_b)$, $U(\mathbf{p}_e)$, $U(\mathbf{v}_b)$, $U(\mathbf{v}_e)$, $U(\mathbf{a}_b)$, $U(\mathbf{a}_e)$. Using formula (34) we derive in Step 1 of the construction the expansions of the control points $\mathbf{h}_0$, $\mathbf{h}_1$, $\mathbf{h}_7$ and $\mathbf{h}_8$.

The squared norms of the boundary derivatives are

$$||\mathbf{v}_0||^2 = ||U(\mathbf{v}_0)||^2 = h^2, \quad ||\mathbf{v}_1||^2 = ||U(\mathbf{v}_1)||^2 = h^2 + 2x_2h^3 + \ldots,$$

i.e., these vectors are space-like for sufficiently small h. Moreover, the quantities $\alpha(\mathbf{t}_0)$ and $\alpha(\mathbf{t}_1)$ (see Lemma 5) have the expansions

$$\alpha(\mathbf{t}_0) = h + \frac{1}{16}(r_2^2 - y_2^2)h^3 + \ldots, \quad \alpha(\mathbf{t}_1) = h + x_2h^2 + \ldots. \tag{41}$$

They are therefore positive for sufficiently small h.

Then restricting ourselves to the case $\mathcal{W}_0 = \cosh(\theta_0) - \sinh(\theta_0)\,\mathbf{e}_2\mathbf{e}_3$, $\mathcal{W}_4 = \cosh(\theta_4) - \sinh(\theta_4)\,\mathbf{e}_2\mathbf{e}_3$ and using (30), we derive in Step 2 the expansions of the control points $\mathcal{A}_0$ and $\mathcal{A}_4$

$$\mathcal{A}_0 = \sinh\theta_0\sqrt{h}\mathbf{e}_1\mathbf{e}_2 + \cosh\theta_0\sqrt{h}\mathbf{e}_3\mathbf{e}_1 + \mathcal{O}\left(h^{3/2}\right), \tag{42}$$

$$\mathcal{A}_4 = \sinh\theta_4\sqrt{h}\mathbf{e}_1\mathbf{e}_2 + \cosh\theta_4\sqrt{h}\mathbf{e}_3\mathbf{e}_1 + \mathcal{O}\left(h^{3/2}\right). \tag{43}$$

Since $||\mathcal{A}_0||^2 = h + \mathcal{O}(h^2)$ and $||\mathcal{A}_4||^2 = h + \mathcal{O}(h^2)$, using formula (30) we derive in Step 3 the expansions of the control points $\mathcal{A}_1$ and $\mathcal{A}_3$

$$\mathcal{A}_1 = \frac{\tau_1\cosh\theta_0}{\sqrt{h}}\mathbf{e}_1\mathbf{e}_2 + \frac{\tau_1\sinh\theta_0}{\sqrt{h}}\mathbf{e}_3\mathbf{e}_1 + \mathcal{O}\left(\sqrt{h}\right), \tag{44}$$

$$\mathcal{A}_3 = \frac{\tau_3\cosh\theta_4}{\sqrt{h}}\mathbf{e}_1\mathbf{e}_2 + \frac{\tau_3\sinh\theta_4}{\sqrt{h}}\mathbf{e}_3\mathbf{e}_1 + \mathcal{O}\left(\sqrt{h}\right). \tag{45}$$

At this stage we can already fix the free parameters τ_1, τ_3. For $h \to 0$ the curve $\mathbf{c}(t)$ converges to $(0,0,0)^\top$ on the whole interval $[0,1]$. Therefore, if the approximation error should converge to 0, the curve $\mathbf{p}_\Phi(t)$ must converge to $(0,0,0)^\top$ on the whole interval $[0,1]$, too. Hence, its hodograph must converge to $(0,0,0)^\top$ and the preimage $\mathcal{A}_\Phi(t)$ must converge to $\mathbf{0}$ on the interval $[0,1]$. This implies that the control points of the preimage, in particular $\mathcal{A}_1$ and $\mathcal{A}_3$ have to converge to $\mathbf{0}$, and therefore τ_1 and τ_3 must vanish.

After setting $\tau_1 = \tau_3 = 0$ we derive in Step 4 the expansion of the control point $\mathcal{A}_2$. First we need to check that the right hand side R of (36) is space-like and that $\alpha(R)$ is positive as h goes to 0. Indeed,

$$||R||^2 = 324(85 + 13\cosh(\theta_0 - \theta_4))^2h^2 + \mathcal{O}(h^3), \alpha(R) = (1530 + 234\cosh(\theta_0 - \theta_4))h + \mathcal{O}(h^2).$$

Then, using (30) we compute that

$$\mathcal{A}_2 = -\frac{5}{4}(\sinh\theta_0 + \sinh\theta_4)\sqrt{h}\mathbf{e}_1\mathbf{e}_2 + \frac{\sqrt{170 + 26\cosh(\theta_0 - \theta_4)} - 5(\cosh\theta_0 + \cos\theta_4)}{4}\sqrt{h}\mathbf{e}_3\mathbf{e}_1 + \mathcal{O}\left(h^{3/2}\right). \tag{46}$$

Finally, in Step 5, using (18)–(19), we get the expansions of the remaining control points $\mathbf{h}_2$, $\mathbf{h}_3$, $\mathbf{h}_4$, $\mathbf{h}_5$ and $\mathbf{h}_6$ of the hodograph. Using (21) we obtain the expansions of the control points of $\mathbf{p}_\Phi(t)$ and of $\mathbf{p}_\Phi(t)$ itself. Comparing the expansion of $\mathbf{p}_\Phi(t)$ with the expansion of $\mathbf{c}$ we obtain

$$\mathbf{p}_\Phi(t) - \mathbf{c}(t) = \begin{pmatrix} ([X - 5Y - 9]\,t^3 - \frac{1}{2}\,[3X - 19Y - 23]\,t^4 + \sum_{i=5}^{9} s_i t^i)h + \mathcal{O}\left(h^2\right) \\ \mathcal{O}\left(h^2\right) \\ \mathcal{O}\left(h^2\right) \end{pmatrix}, \tag{47}$$

where

$$X = \cosh(\theta_0)\sqrt{170 + 26\,\cosh(\theta_0 - \theta_4)} \text{ and } Y = \cosh(\theta_0 - \theta_4). \tag{48}$$

Therefore the approximation error converges to 0 only as $\mathcal{O}(h)$ unless

$$X - 5Y - 9 = 0 \text{ and } 3X - 19Y - 23 = 0, \tag{49}$$

which holds only for $X = 14$ and $Y = 1$. This implies $\theta_0 = \theta_4 = 0$ and thus $\mathcal{W}_0 = \mathcal{W}_4 = \mathbf{1}$.

After setting $\theta_0 = \theta_4 = 0$ the Taylor expansion of $\mathbf{p}_\Phi(t)$ simplifies enormously and matches the Taylor expansion of $\mathbf{c}(t)$ up to h^5. □

5. Applications and examples

In this section we discuss applications of the interpolation algorithm designed in Section 3 and demonstrate them on several examples.

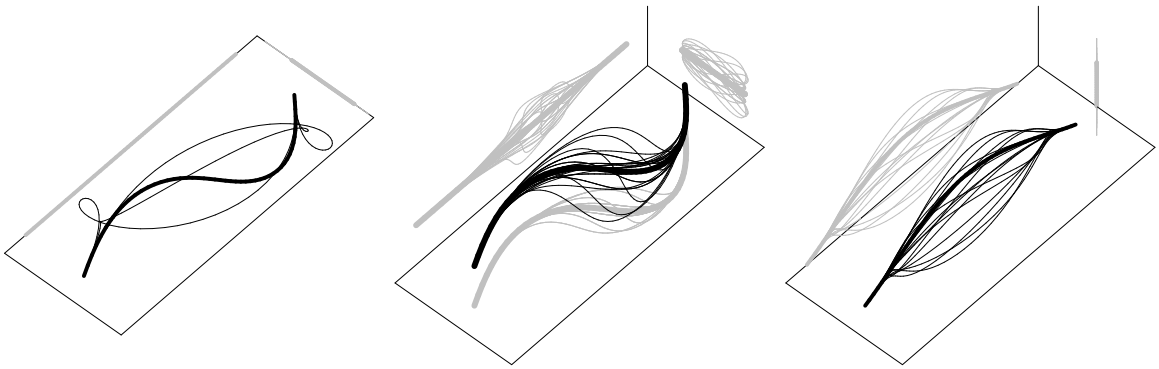

Figure 1: Interpolation of planar data. The best interpolant $\mathbf{p}_{[\mathbf{1},0,0,\mathbf{1}]}(t)$ is depicted in bold.

5.1. C^2 interpolation and curve conversion

We start with interpolating given C^2 Hermite boundary data by an MPH curve and a conversion of an analytic space-like curve (considered as a segment of MAT) into a C^2 MPH spline.

Example 1. We apply the C^2 Hermite interpolation algorithm to the data

$$\mathbf{p}_b = (0,0,0)^\top,\ \mathbf{p}_e = (1,0,0)^\top,\ \mathbf{v}_b = (1,1,0)^\top,\ \mathbf{v}_e = (2,1,0)^\top,\ \mathbf{a}_b = (1,2,0)^\top,\ \mathbf{a}_e = (1,2,0)^\top. \tag{50}$$

Since these data are planar (they lie in a space-like plane), a natural question is to ask which interpolants preserve this planarity. According to Theorem 1, the interpolant $\mathbf{p}_{[\mathbf{1},0,0,\mathbf{1}]}(t)$ is planar. However, more interpolants can be planar. We present the following result without proof: Let $\mathbf{v}_b + \mathbf{v}_e$ be a space-like vector and the input data lie in a plane π. For space-like planes π the four interpolants $\mathbf{p}_{[\mathcal{W}_0,0,0,\mathcal{W}_4]}(t)$, $\mathcal{W}_0, \mathcal{W}_4 \in \{\mathbf{1}, -\mathbf{1}\}$ are planar. If π is time-like, then we obtain 16 planar interpolants $\mathbf{p}_{[\mathcal{W}_0,0,0,\mathcal{W}_4]}(t)$, $\mathcal{W}_0, \mathcal{W}_4 \in \{\mathbf{1}, -\mathbf{1}, \mathbf{e}_3\mathbf{e}_1, -\mathbf{e}_3\mathbf{e}_1\}$ from the interpolation scheme.

The four planar interpolants to the data (50) are shown in Fig. 1, left. Note that since the input data lie in a space-like plane, the four interpolants match the four planar interpolants given by the C^2 PH interpolation scheme, cf. Theorem 3.11 of [23]. Fig. 1, middle, illustrates the influence of the parameters $\mathcal{W}_0, \mathcal{W}_4$. It depicts several members of the family $\mathbf{p}_{[\mathcal{W}_0,0,0,\mathcal{W}_4]}(t)$. Finally, in Fig. 1, right, we show the 16 planar interpolants to a given data lying in a time-like plane. In all three figures the best interpolant $\mathbf{p}_{[\mathbf{1},0,0,\mathbf{1}]}(t)$ is depicted in bold and projections to auxiliary planes are shown in gray.

Example 2. The interpolation algorithm can be used to convert any space-like analytic curve into a C^2 MPH spline. We start with a curve $\mathbf{c}(t)$ defined on $[0,1]$. Using uniform subdivision, we split the unit interval into 2^n subdomains, for each of which we compute the MPH interpolant $\mathbf{p}[\mathbf{1},0,0,\mathbf{1}](t)$. We remark that using an adaptive subdivision would reduce the number of interpolants required in order to achieve a sufficiently small approximation error.

The order of convergence is demonstrated by the following example, see Fig 2. Consider the curve segment

$$\mathbf{c}(t) = (0.25t\cos(8t+0.7), 0.85\sinh(t), 1-\cosh(t-0.5)/\cosh(0.5))^\top,\ t \in [0,1]. \tag{51}$$

The approximation error (based on point sampling estimation) along with its improvement in the first subinterval is summarized in Table 1. Note that the ratios of subsequent errors converge to 64, as Theorem 2 predicts. Similar errors with ratios converging to 64 were obtained for the approximation of the two envelope branches as well.

5.2. Medial axis approximation

Now we address the problem of approximating the MAT of a given planar domain by a C^2 MPH spline. MAT has a structure of a geometric graph; it consists of curve segments which are pieced together at the graph vertices [4]. We will now focus only on approximation of individual segments. A discussion of end points and bifurcation points of the MAT will be the subject of a separate publication.

Table 1: Numerical results obtained in Example 2 by uniform refinement.

segments	error	ratio	segments	error	ratio	segments	error	ratio
1	$2.367 \cdot 10^{-1}$	–	8	$1.162 \cdot 10^{-5}$	40.23	64	$5.945 \cdot 10^{-11}$	66.51
2	$1.025 \cdot 10^{-2}$	23.09	16	$2.480 \cdot 10^{-7}$	46.85	128	$9.028 \cdot 10^{-13}$	65.85
4	$4.675 \cdot 10^{-4}$	21.93	32	$3.954 \cdot 10^{-9}$	62.72	256	$1.388 \cdot 10^{-14}$	65.04

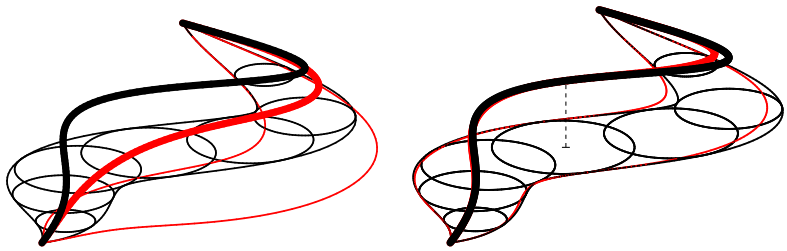

Figure 2: Approximating a space-like analytic curve (black) by a C^2 MPH spline (red). Two steps of subdivision are depicted. Several MAT circles are shown along with the corresponding envelopes.

An important advantage of using MPH curves for MAT approximation is the efficient offset computation including inner offset trimming. In fact, only the parts of the MAT for which the corresponding disk radius (last coordinate of the MAT) is smaller than the offset distance (or cutting tool radius in practice) need to be removed, see Fig. 3, left.

In order to obtain suitable C^2 data for Hermite interpolation from a planar domain Ω, we apply the following elegant

Theorem 3. *Let $M \in \mathrm{MAT}(\Omega)$ correspond to a disc touching $\partial\Omega$ at C and D, see Fig. 3, right. Consider the two light cones L_C, L_D which are constructed over the osculating circles of $\partial\Omega$ at C and D and which contain M. Then L_C, L_D intersect in the osculating Minkowski circle of $\mathrm{MAT}(\Omega)$ at M.*

PROOF. It is known, that the intersection of L_C and L_D is a second degree approximation to $\mathrm{MAT}(\Omega)$ at M, cf. Proposition 2 of [17]. It therefore suffices to show that the intersection of the cones is a Minkowski circle, i.e., a planar curve of a constant Minkowski distance from a certain center.

The implicit equations of L_C and L_D have identical quadratic terms. Thus their intersection decomposes into a common conic section in the plane at infinity and another conic, which lies in the plane π, whose equation is obtained as the difference of the equations of the cones. This section is a Minkowski circle, because it is a planar section of a light cone. Indeed, any light cone is a Minkowski sphere with zero diameter. More precisely, if V is the vertex of L_C and $S \in \pi$ the point closest to V, then we have for any point X of the section $||X - S||^2 = -||P - S||^2 = const.$ and the section is a Minkowski circle with center S. If the plane is space-like, the osculating Minkowski circle is a Euclidean ellipse. If the plane is time-like, we get a Euclidean hyperbola. The two cones never intersect in a Euclidean parabola. They however may share a common light-like line, which can be understood as a Minkowski circle with zero radius. □

Now we are ready to describe the algorithm for the medial axis approximation. We do not want to enter into a discussion on the topology of the MAT and therefore we restrict ourselves only to approximation of curve segments of the MAT whose points correspond to maximal circles having precisely two contact points with $\partial\Omega$.

1. Sample a suitable sequence of points C_i on $\partial\Omega$.
2. For each C_i find its corresponding D_i sharing the same maximal disc.
3. For each pair C_i, D_i find the point M_i of $\mathrm{MAT}(\Omega)$.
4. Intersect L_{C_i} with L_{D_i} and parameterize the resulting Minkowski circle c_i.
5. Sample C^2 Hermite data from c_i at M_i and apply the C^2 interpolation scheme to consecutive points M_i, M_{i+1}.
6. Piece the resulting MPH curves together, obtaining an MPH spline approximation of $\mathrm{MAT}(\Omega)$.

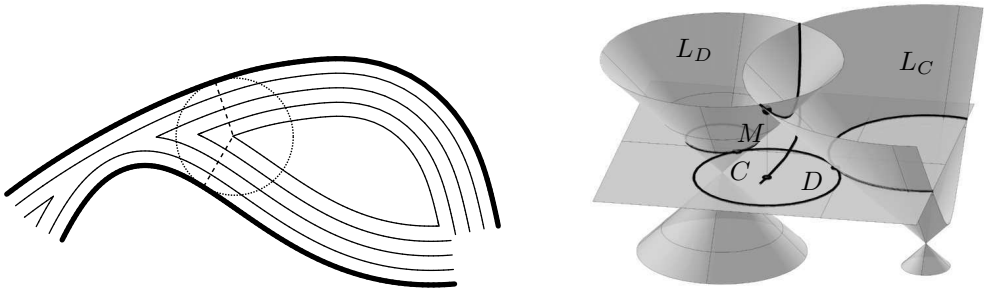

Figure 3: Left: Inner offset trimming using the MAT. Right: Intersection of cones over osculating circles 3.

Table 2: Numerical results obtained in Example 3 for the boundary curve $\mathbf{q}(t)$.

segments	error	ratio	segments	error	ratio	segments	error	ratio
1	$3.503 \cdot 10^{-2}$	–	8	$6.425 \cdot 10^{-6}$	35.06	64	$4.882 \cdot 10^{-11}$	64.68
2	$1.660 \cdot 10^{-3}$	21.10	16	$1.884 \cdot 10^{-7}$	34.11	128	$7.508 \cdot 10^{-13}$	65.02
4	$2.252 \cdot 10^{-4}$	7.37	32	$3.158 \cdot 10^{-9}$	59.66	256	$1.161 \cdot 10^{-14}$	64.68

Steps 1–4 are simple geometric tasks that can be solved using various algorithms, which we do not discuss in the present paper. Step 5 is realized using the interpolant $\mathbf{p}_{[\mathbf{1},0,0,\mathbf{1}]}(t)$ thoroughly discussed above.

Example 3. In this example we apply the C^2 MPH approximation algorithm to the medial axis transform approximation of a planar region bounded by two curve segments, see Fig. 4. The segments of the region boundary are polynomial quartics $\mathbf{q}(t)$, $\mathbf{r}(t)$ given by their Bézier control points

$$\begin{aligned} &Q_0 = (-1.7, 0.8)^\top,\ Q_1 = (-0.5, 0.9)^\top,\ Q_2 = (0, 0)^\top,\ Q_3 = (0.5, -0.5)^\top,\ Q_4 = (1, 0.5)^\top, \\ &R_0 = (-2, 0.4)^\top,\ R_1 = (-1.7, -1.1)^\top,\ R_2 = (-0.8, -1)^\top,\ R_3 = (0.5, -0.5)^\top,\ R_4 = (1.4, 0.2)^\top. \end{aligned} \tag{52}$$

Following the steps of the algorithm, we first sample points from $\mathbf{q}(t)$. Then we compute the corresponding points on $\mathbf{r}(t)$ and MAT using a suitable scheme for finding maximal inscribed discs. Next, we parameterize (using Minkowski arc-length) the Minkowski circles given by the intersection of the light-cones described in Theorem 3. These provide us with C^2 data which we in turn use for constructing the MPH spline approximation of the original domain's MAT. Finally, using the envelope formula (11) we compute rational PH spline approximations of the domain boundary.

The error obtained for the approximation of $\mathbf{q}(t)$ is summarized in Table 2. Same order of error improvement was achieved for $\mathbf{r}(t)$, too. Note that the error ratios tend to 64, suggesting that the proposed method possesses approximation order 6 not only for the approximation of MAT, but for the domain boundary as well. A detailed analysis of the exact approximation order is a matter of future research.

6. Conclusion

We have fully solved the problem of C^2 Hermite interpolation by MPH nonics in the space $\mathbb{R}^{2,1}$. The use of a Clifford algebra formalism revealed that there is a structural analogy of this problem to the Euclidean case, technical details remaining different due to the particularities of the Minkowski metric. We have identified one interpolant particularly well suited for applications and used it for approximation of individual branches of MAT. In the future we plan to include this approach into an algorithm for approximation of the whole MAT of closed domains and treat stability and topological questions.

Acknowledgment

Zbyněk Šír was supported by the project MSM 0021620839 of the Czech Ministry of Education and by the project no. 201/08/0486 of the Czech Science Foundation.

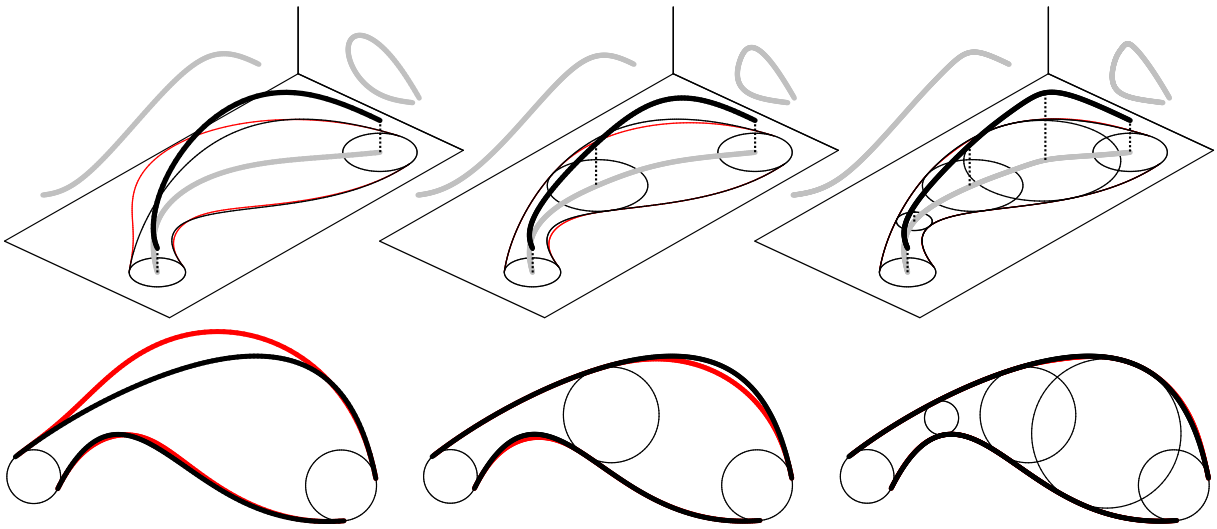

Figure 4: Three steps of subdivision applied to MAT approximation. Associated domain boundary approximations are depicted in red. The MAT discs at sampled points are shown as well.

References

[1] Aurenhammer F., Aichholzer O., Hackl T., Jüttler B., Oberneder M., and Šír, Z., Structural and computational advantages of circular boundary representations, in Algorithms and Data Structures, Lecture Notes in Computer Science vol. 4619, Berlin 2007, 374–385.

[2] Chazal F., and Soufflet R., Stability and finiteness properties of medial axis and skeleton, J. Dynamical and Control Systems, 10 (2004), 149–170.

[3] Cho H. Ch., Choi, H. I., Kwon S.–H., Lee D. S., and Wee N.–S., Clifford algebra, Lorentzian geometry and rational parametrization of canal surfaces, Comp. Aided Geom. Design, 21 (2004), 327–339.

[4] Choi, H. I., Choi, S. W., and Moon, H. P., Mathematical theory of medial axis transform, Pacific J. Math., 181(1) (1997), 57–88.

[5] Choi, H. I., Farouki, R. T., Kwon, S.-H., and Moon, H. P., Topological Criterion for Selection of Quintic Pythagorean-Hodograph Hermite Interpolants, Comput. Aided Geom. Design, 25 (6) (2008), 411–433.

[6] Choi, H. I., Han, Ch. Y., Moon, H. P., Roh, K. H., and Wee, N. S., Medial axis transform and offset curves by Minkowski Pythagorean hodograph curves, Comp.–Aided Design, 31 (1999), 59–72.

[7] Choi, H. I., Lee, D. S., and Moon, H. P., Clifford algebra, spin representation and rational parameterization of curves and surfaces, Advances in Computational Mathematics, 17 (2002), 5–48.

[8] Degen, W. L. F., Exploiting curvatures to compute the medial axis for domains with smooth boundary, Comp. Aided Geom. Design, 21 (2004), 641–660.

[9] Farouki, R. T. (2002), Pythagorean hodograph curves, in G. Farin, J. Hoschek and M.-S. Kim (eds.), Handbook of Computer Aided Geometric Design, North-Holland, Amsterdam, 405–427.

[10] Farouki, R. T. (2008), Pythagorean-Hodograph Curves: Algebra and Geometry Inseparable, Springer, Berlin.

[11] Farouki, R. T., al-Kandari, M., and Sakkalis, T, Hermite interpolation by rotation–invariant spatial Pythagorean–hodograph curves, Advances in Computational Mathematics, 17 (2002), 369–383.

[12] Farouki, R. T., Han, Ch. Y., Manni, C., and Sestini, A., Characterization and construction of helical polynomial space curves, J. Comput. Appl. Math. 162 (2004), 365–392.

[13] Farouki, R. T. and Sakkalis T., Pythagorean hodographs, IBM Journal of Research and Development, 34 (1990), 736–752.

[14] Hoschek, J. and Lasser, D. (1996), Fundamentals of Computer Aided Geometric Design, AK Peters, Wellesley MA.

[15] Jüttler, B. and Mäurer, C., Cubic Pythagorean Hodograph Spline Curves and Applications to Sweep Surface Modeling, Comp.–Aided Design, 31 (1999), 73–83.

[16] Kosinka, J. and Jüttler, B., Cubic Helices in Minkowski Space, Sitzungsber. Oesterr. Akad. Wiss., Abt. II., 215 (2006), 13–35.

[17] Kosinka, J. and Jüttler, B., G^1 Hermite Interpolation by Minkowski Pythagorean Hodograph Cubics, Comp. Aided Geom. Design, 23 (2006), 401–418.

[18] Kosinka, J. and Jüttler, B., C^1 Hermite Interpolation by Pythagorean Hodograph Quintics in Minkowski space, Advances in Applied Mathematics 30 (2009), 123–140.

[19] Kim, G.–I. and Ahn M.–H., C^1 Hermite interpolation using MPH quartic, Comp. Aided Geom. Design, 20 (2003), 469–492.

[20] Moon, H. P., Minkowski Pythagorean hodographs, Comp. Aided Geom. Design, 16 (1999), 739–753.

[21] Pottmann, H. and Peternell, M., Applications of Laguerre geometry in CAGD, Comp. Aided Geom. Design, 15 (1997), 165–186.

[22] Šír, Z. and Jüttler, B. (2005), Spatial Pythagorean Hodograph Quintics and the Approximation of Pipe Surfaces, The Mathematics of Surfaces XI, Springer Lecture Notes on Computer Science vol. 3604, Berlin, 364–380.

[23] Šír, Z. and Jüttler, B., C^2 Hermite interpolation by spatial Pythagorean hodograph curves, Math. Comp., 76 (2007), 1373–1391.